Title

The selective estrogen receptor modulator raloxifene mitigates the effect of all-trans-retinal toxicity in photoreceptor degeneration

Journal

Journal of Biological Chemistry, 294(24)

ISSN

0021-9258

Authors

Getter, Tamar
Suh, Susie
Hoang, Thanh
et al.

Publication Date

2019-06-01

DOI

10.1074/jbc.ra119.008697

The selective estrogen receptor modulator raloxifene mitigates the effect of all-*trans*-retinal toxicity in photoreceptor degeneration

Received for publication, April 1, 2019, and in revised form, May 8, 2019 Published, Papers in Press, May 9, 2019, DOI 10.1074/jbc.RA119.008697

Tamar Getter[‡§1], **Susie Suh**[‡§], **Thanh Hoang**[¶], **James T. Handa**[‖2], **Zhiqian Dong**[**], **Xiuli Ma**[**], **Yuanyuan Chen**[‡‡§§], **Seth Blackshaw**[¶], and **Krzysztof Palczewski**[‡§3]

From the [‡]*Gavin Herbert Eye Institute, Department of Ophthalmology, University of California, Irvine, California 92697, the* [§]*Department of Pharmacology, Case Western Reserve University, Cleveland, Ohio 44106, the* [¶]*Solomon H. Snyder Department of Neuroscience, Johns Hopkins University School of Medicine, Baltimore, Maryland 21205, the* [‖]*Wilmer Eye Institute, Department of Ophthalmology, Johns Hopkins University School of Medicine, Baltimore, Maryland 21287, **Polgenix Inc., Irvine, California 92617, the* [‡‡]*Department of Ophthalmology, School of Medicine, University of Pittsburgh, Pittsburgh, Pennsylvania 15260, and the* [§§]*McGowan Institute of Regenerative Medicine, University of Pittsburgh, Pittsburgh, Pennsylvania 15213*

Edited by Henrik G. Dohlman

The retinoid cycle is a metabolic process in the vertebrate retina that continuously regenerates 11-*cis*-retinal (11-*cis*RAL) from the all-*trans*-retinal (atRAL) isomer. atRAL accumulation can cause photoreceptor degeneration and irreversible visual dysfunction associated with incurable blinding retinal diseases, such as Stargardt disease, retinitis pigmentosa (RP), and atrophic age-related macular degeneration (AMD). The underlying cellular mechanisms leading to retinal degeneration remain uncertain, although previous studies have shown that atRAL promotes calcium influx associated with cell apoptosis. To identify compounds that mitigate the effects of atRAL toxicity, here we developed an unbiased and robust image-based assay that can detect changes in intracellular calcium levels in U2OS cells. Using our assay in a high-throughput screen of 2,400 compounds, we noted that selective estrogen receptor modulators (SERMs) potently stabilize intracellular calcium and thereby counteract atRAL-induced toxicity. In a light-induced retinal degeneration mouse model (*Abca4*$^{-/-}$*Rdh8*$^{-/-}$), raloxifene (a benzothiophene-type scaffold SERM) prevented the onset of photoreceptor apoptosis and thus protected the retina from degeneration. The minor structural differences between raloxifene and one of its derivatives (Y 134) had a major impact on calcium homeostasis after atRAL exposure *in vitro*, and we verified this differential impact *in vivo*. In summary, the SERM raloxifene has structural and functional neuroprotective effects in the retina. We propose that the highly sensitive image-based assay developed here could be applied for the discovery of additional drug candidates preventing photoreceptor degeneration.

Retinal degeneration associated with abnormal retinoid metabolism and exposure to bright light can cause visual dysfunction and retinal photoreceptor damage in humans and experimental animals (1). Vision at the molecular level relies on a metabolic pathway that continuously regenerates 11-*cis*-retinal (11-*cis*RAL)[4] from its all-*trans*-retinal (atRAL) isomer (2). atRAL is a photoproduct released from bleached rhodopsin, and its efficient clearance from retinal rod outer segment (ROS) discs and isomerization to 11-*cis*-retinal by the visual cycle enzymes are essential for the effective renewal of light-sensitive visual pigments and maintenance of rod photoreceptor homeostasis (3, 4). Inadequate clearance of atRAL, for example, can result in the formation of diretinoid-pyridinium-ethanolamine (A2E), a condensation product of atRAL and a surrogate marker for toxic retinoids (5). Humans affected by age-related macular degeneration (AMD), Stargardt disease, retinitis pigmentosa (RP), or other retinal diseases associated with the abnormal accumulation of atRAL condensation products undergo retinal degeneration, which eventually culminates in vision loss (5, 6). Currently, there are only limited treatments for retinal degeneration caused by this metabolic defect. Even in the presence of a viable retinoid cycle, A2E and other toxic atRAL condensation products accumulate during normal aging

This research was supported in part by NEI, National Institutes of Health, Grants R24EY024864 and R24EY027283 (to K. P.), EY024992 (to Y. C.), T32GM007250 and F30EY029136-01A1 (to S. S.), and R01EY027691 (to J. T. H.); an unrestricted grant from Research to Prevent Blindness to the Department of Ophthalmology at the University of California (Irvine, CA); the Canadian Institute for Advanced Research (CIFAR); and the Alcon Research Institute (ARI). K. P. is Chief Scientific Officer at Polgenix, Inc. Z. D. and X. M. are employees of Polgenix, Inc. The content is solely the responsibility of the authors and does not necessarily represent the official views of the National Institutes of Health.

This article contains Table S1 and Figs. S1–S6.

[1] To whom correspondence may be addressed: Gavin Herbert Eye Institute, Dept. of Ophthalmology, University of California, Irvine, CA 92657. Tel.: 949-824-5154; E-mail: tgetter@uci.edu.

[2] Robert Bond Welch Professor.

[3] Leopold Chair of Ophthalmology. To whom correspondence may be addressed: Gavin Herbert Eye Institute, Dept. of Ophthalmology, University of California, Irvine, CA 92657. Tel.: 949-824-6527; E-mail: kpalczew@uci.edu.

[4] The abbreviations used are: 11-*cis*RAL, 11-*cis*-retinal; AM, acetoxymethyl; atRAL, all-*trans*-retinal; atROL, all-*trans*-retinol; CCB, calcium channel blocker; 9-*cis*RAL, 9-*cis*-retinal; A2E, diretinoid-pyridinium-ethanolamine; ERG, electroretinography; ERα, estrogen receptor α (gene *Esr1*); ERβ, estrogen receptor β (gene *Esr2*); ER, estrogen receptor; GPER30, G protein–coupled estrogen receptor 1 (gene *Gper1*); HTS, high-throughput screen; i.p., intraperitoneal; mER, membrane estrogen receptor; OCT, optical coherence tomography; SD-OCT, spectral domain OCT; ONL, outer nuclear layer; RPE, retinal pigmented epithelial; RP, retinitis pigmentosa; ROS, rod outer segment; SLO, scanning laser ophthalmoscopy; SERM, selective estrogen receptor modulator; DMEM, Dulbecco's modified Eagle's medium; S/B, signal/background; scRNA, single-cell RNA.

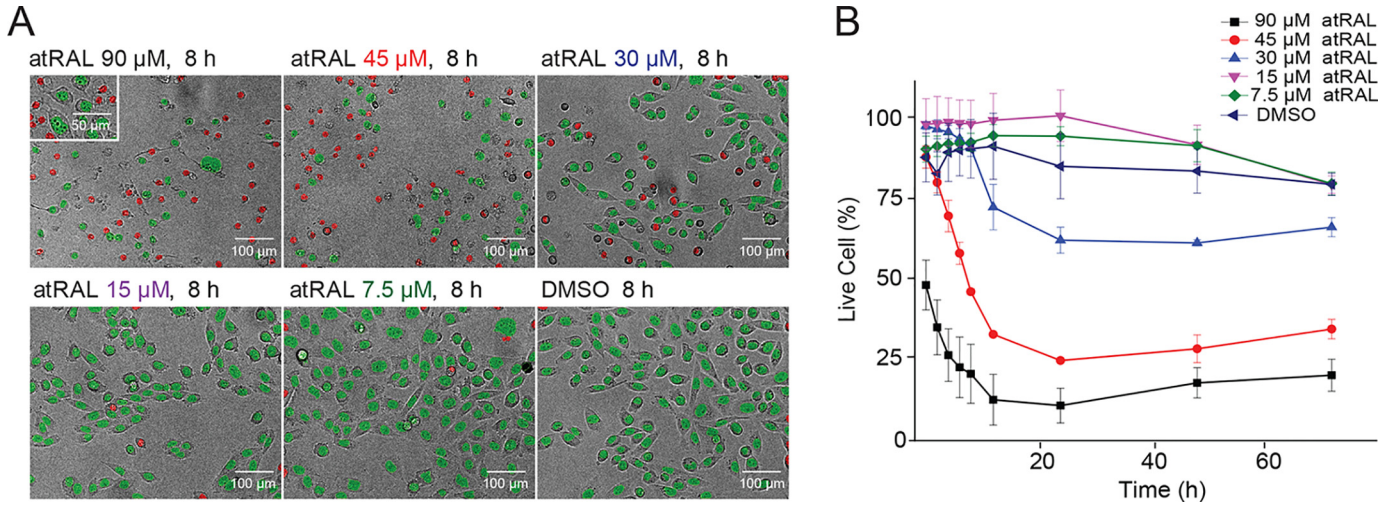

Figure 1. Image-based evaluation of nuclear morphology in U2OS cells after atRAL exposure. *A*, apoptotic changes in nuclear morphology observed by Hoechst 33342 staining. Shown are representative images of the nuclear morphology counterstained with Hoechst 33342 after an 8-h incubation with atRAL at 7.5, 15, 30, 45, and 90 μM or with DMSO. Nuclear morphology was assessed with Harmony® high-content imaging and analysis software. *Red*, dead cells, nuclear area $<$ 200 pixels^2; *green*, live cells, nuclear area $>$ 200 pixels^2. *B*, nuclear morphology quantification monitored through 3 days post-atRAL at 7.5, 15, 30, 45, and 90 μM or with DMSO. *Error bars*, S.D. of triplicate readings.

(7, 8). It is postulated that the mechanism of cell death induced by atRAL involves a prolonged elevation of intracellular calcium, which in turn triggers mitochondria-associated cell death (9, 10). Our previous studies showed that pharmacological treatments that either scavenge free atRAL (11) or prevent rod photoreceptor cells from atRAL-induced intracellular calcium influx protect the retina from light damage (6, 12). However, potent pharmacological targets and drug treatments that effectively protect photoreceptors from calcium influx are limited. Thus, the goal of this investigation was to identify Food and Drug Administration–approved drugs that preserve calcium homeostasis and repurpose their known targeted mechanistic pathways to protect the retina from atRAL toxicity (9).

In this study, we developed an image-based high-throughput screen (HTS) assay to identify hit compounds that maintain normal calcium homeostasis after exposure to atRAL, without impairing the retinoid cycle required by the mammalian visual system. Such an image-based HTS assay with a unique measurement of calcium as an indicator of insult from reactive aldehydes is of substantial value not only to this study, but also a useful tool to the vision community for studies related to the calcium pathway. Followed by comprehensive medicinal chemistry and *in vivo* studies, we identified a group of potent compounds that effectively protects the retina from light-induced atRAL toxicity. More importantly, the common triphenylethylene parent compounds revealed an important target for therapies maintaining calcium homeostasis in the retina. Nonsteroidal selective estrogen receptor modulators (SERMs), clomiphene (13–15) and toremifene (16, 17), well-established and widely used drugs that are known to exert agonist and antagonist effects (18), were identified as potential therapeutics against photoreceptor degeneration. Whereas these drugs have shown to be estrogenic in some species, they are anti-estrogenic in others, leading to conflicting effects regarding the exact mechanism of action. There are currently two main chemical classes of SERMs approved for clinical use, triphenylethylene (19) and a benzothiophene derivative (20). However, the effect of SERMs on photoreceptors is not completely understood. Estrogen receptors (ERs) consist of two subtypes: nuclear receptors that mediate their effects via gene transcriptional regulation (21) and nonnuclear receptors that are membrane estrogen receptors (mERs) (22) that alter cell signaling via the modulation of intracellular signaling cascades associated with calcium homeostasis (23). In this study, we subjected these drugs to an *in vitro* calcium homeostasis evaluation and an *in vivo* light-induced damage assessment. Our findings likely will yield new targets for drug intervention in the prevention and/or progression of retinal degenerative diseases.

Results

atRAL-induced cell death

To ensure the robustness and sensitivity of our HTS assay, we initially evaluated the optimal concentration and treatment time of atRAL, whereby an insult was sufficient to elevate intracellular calcium levels without causing extreme cytotoxicity. We treated human bone osteosarcoma epithelial (U2OS) cells with 7.5, 15, 30, 45, and 90 μM atRAL and monitored cell viability over 72 h. Cell viability was analyzed by quantifying dying and live cells by nuclear morphologic changes of U2OS cells exposed to atRAL (Fig. 1). We showed that atRAL decreased U2OS cell survival as a function of both exposure time and atRAL concentration. At a higher concentration (45 or 90 μM), atRAL induced severe cellular toxicity even with shorter exposure time (8 h). In contrast, at a lower concentration (7.5, 15, or 30 μM), atRAL showed a minor effect on cell survival with longer periods of exposure (72 h). To confirm this result, we used a CellTiter-Glo luminescent cell viability assay, which measures the number of viable cells in culture based on the quantification of ATP. Cells were exposed to atRAL concentrations of 15, 30, and 60 μM for 1–24 h (Fig. S1). With 1 h of incubation, ATP levels remained stable at all concentration levels, but a longer incubation with atRAL dramatically decreased the ATP concentrations in a dose-dependent manner, indicating a reduced

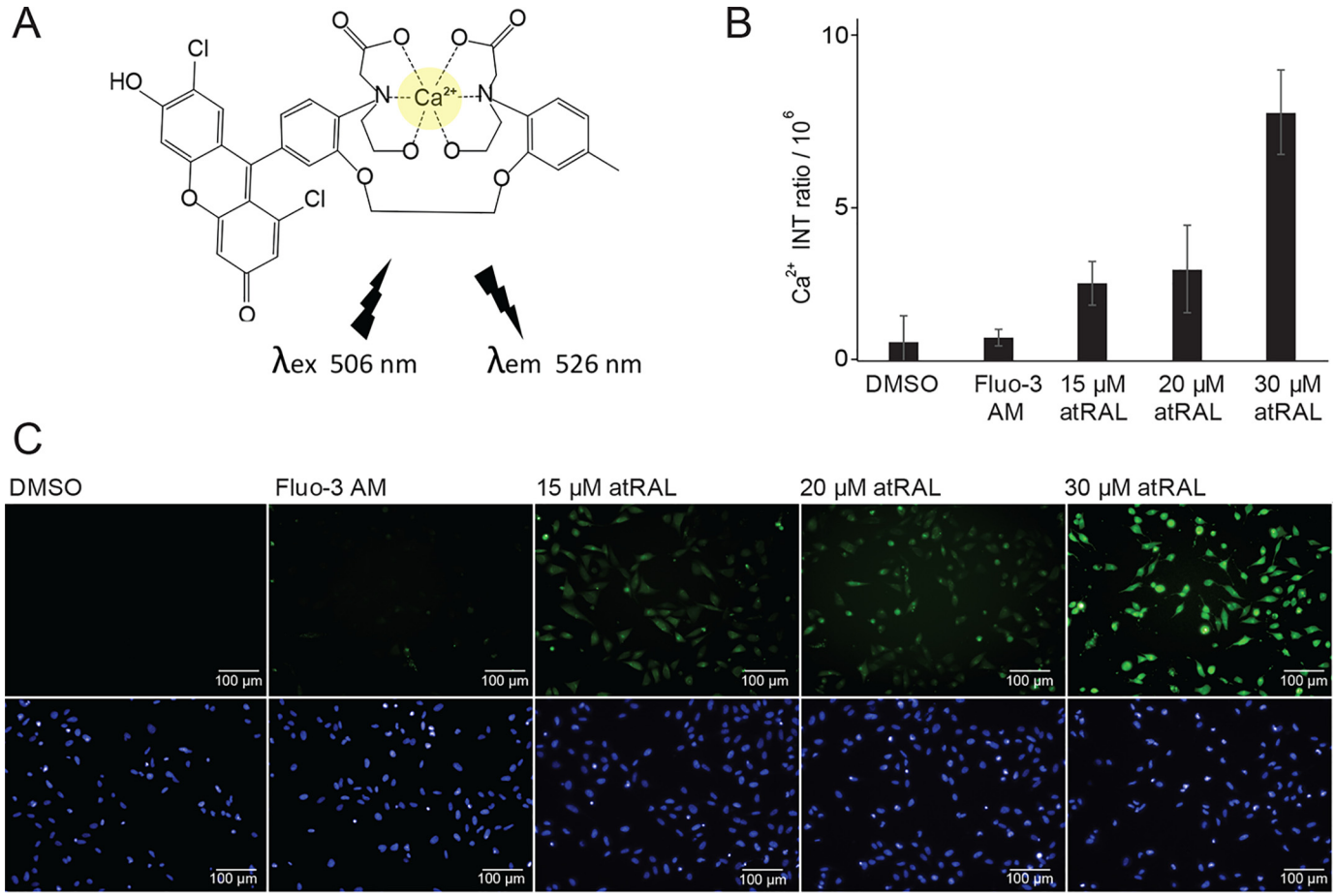

Figure 2. Exposure to atRAL rapidly increases intracellular calcium. *A*, chemical structure of fluorescent fluo-3–Ca^{2+} complex with an excitation at 506 nm and emission at 526 nm. *B*, quantification of fluo-3–Ca^{2+} complex fluorescence intensity (*INT*) ratio responses in U2OS cells caused by 15, 20, and 30 μM atRAL exposure for 15 min. Ca^{2+} intensity was obtained by a subtraction of fluo-3 intensity in the background (mean) from fluo-3 intensity within cells (mean). *C*, representative fluorescence images of fluo-3 AM (*green*, calcium indicator) and Hoechst 33342 (*blue*, nuclear marker) in U2OS cells treated with 15, 20, and 30 μM atRAL. *Error bars*, S.D. of triplicate readings.

number of viable cells with longer than 1 h atRAL incubation. Based on these results, we proceeded with our HTS assay using atRAL at a concentration of 30 μM with an incubation time of less than 1 h.

atRAL-induced cellular calcium influx

To quantify atRAL-induced calcium influx, which triggers cell apoptosis (24, 25), we visualized intracellular calcium in U2OS cells by using the cell-permeable dye fluo-3 AM with a high-content imaging system (Fig. 2). atRAL increased the fluorescent intensity of cells loaded with fluo-3 in a dose-dependent manner after only 15 min of exposure time, indicating a rapid increase in intracellular calcium concentration. Next, we measured the effects of other aldehyde-derived retinoids (11-*cis*RAL, 9-*cis*-retinal (9-*cis*RAL), all-*trans*-retinol (atROL), and A2E) on intracellular calcium levels (Fig. 3*A*). All aldehyde derivatives and A2E demonstrated elevated intracellular calcium, whereas atROL had no significant effect, showing normal calcium homeostasis, suggesting that all free aldehyde derivatives of retinoids are cytotoxic. To confirm that atRAL toxicity is indeed associated with its aldehyde moiety, we tested whether free-aldehyde scavenger compounds, primary amine-containing drugs MB-001 and emixustat, affect the atRAL-induced calcium influx. Primary amine drugs formed a Schiff base with the aldehyde derivative of atRAL (Fig. 3*B*), preventing the reactivity of atRAL from reaching toxic levels that trigger calcium influx (26). Our assay showed that MB-001 and emixustat lowered the intracellular calcium levels in a dose-dependent manner, whereas MB-002 lacking a primary amine moiety had no protective effect (Fig. 3*C*). In addition, we tested atRAL-dependent cell viability on six different cell lines, namely human retinal pigment epithelial cells (ARPE-19), mouse embryonic fibroblast cells (NIH-3T3), human embryonic kidney 293 cells (HEK-293), human breast cancer cells (MCF-7), Chinese hamster ovary cells, and U2OS cells. Each of these demonstrated a rise in intracellular calcium levels after atRAL exposure and dose-dependent cellular apoptosis (Fig. S2), suggesting that the atRAL-dependent induction of cytotoxicity through elevation of intracellular calcium levels occurs in a broad range of cell types.

HTS assay monitoring intracellular calcium influx

To discover effective compounds that mitigate atRAL toxicity, we applied an image-based HTS assay that measures intracellular levels of calcium using cell-permeable fluo-3 AM fluorescence as an indicator of cellular stress. We optimized our

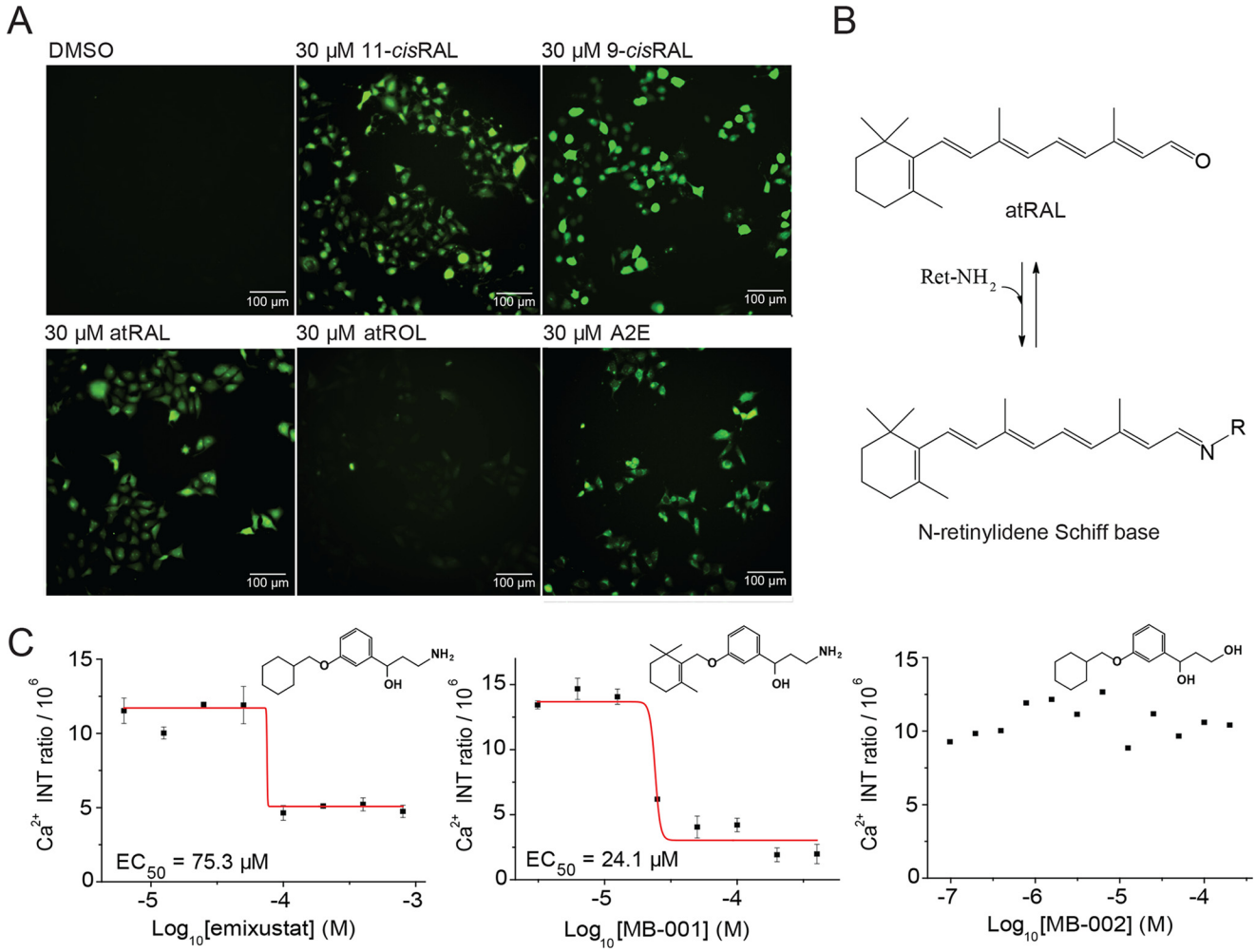

Figure 3. Retinoid and primary amine effects on intracellular calcium. *A*, cellular calcium imaging after treatment with DMSO or with 30 μM 11-*cis*RAL, 9-*cis*RAL, atRAL, atROL, and A2E. *B*, condensation reaction of atRAL with primary amines resulting in *N*-retinylidene Schiff base formation. *C*, dose–response effects of emixustat, MB-001, and MB-002 on calcium influx due to atRAL quenching. The dose–response curves of primary amine compounds emixustat and MB-001 along with the hydroxyl-conjugated MB-002 compound are plotted by intensity (*INT*) ratio of the fluo-3–Ca^{2+} complex. Concentrations tested were in the range of 0.8–400 μM. *Error bars*, S.D. of triplicate readings.

HTS assay with the time course and dose-response evaluations for calcium channel blocker (CCB) treatment prior to atRAL exposure (Fig. 4*A*). As a positive control, we selected nilvadipine, a CCB that demonstrated protective effects on photoreceptor degeneration in animal models of RP (27–30). In our system, pretreatment with nilvadipine to obtain normal calcium levels after atRAL exposure significantly reduced the intracellular calcium responses as compared with the DMSO control tested in a dose-dependent manner due to the ability of CCB to reduce calcium excess to cells (Fig. 4*B*). A total of 2,400 compounds, including 1,600 Food and Drug Administration–approved drugs and 800 natural substances and pharmacologically active compounds formatted as 10 mM stocks in DMSO, were screened at a final calibrated concentration of 11 μM (Fig. 4, *C* and *D*). The screen identified an initial 37 hit compounds, from which we selected 25 compounds that best represented the desired structural diversity and druglike properties. All compounds were tested over a range of 10 concentrations in triplicate to determine their EC_{50} values. Twelve dose-dependent hits were identified with EC_{50} values of 1–45 μM (Fig. 3).

Effect of SERMs on intracellular calcium influx

Interestingly, two of the 12 identified hit compounds from our HTS assay shared a triphenylethylene parent scaffold acting as SERMs. Clomiphene and toremifene in Fig. 5*A*, exhibiting a positive calcium balance output after treatment with EC_{50} values of 25.5 and 29.2 μM, respectively, were of particular interest due to their structural similarity to tamoxifen (31, 32). Tamoxifen, another member of the triphenylethylene SERMs, has previously been reported for its photoreceptor protective effect by significantly improving retinal structure, light responses, and visual behavior (33). To validate that the dose-dependent responses for both clomiphene and toremifene were not due to the interaction of compounds with the calcium dye, we developed a noncellular counterscreen assay using the hydrolyzed form of fluo-3 AM ester (fluo-3). Fluo-3 permeates cell membranes as an ester and is hydrolyzed in the cell to its calcium-sensitive acidic form. To probe the activity of the dye in a noncellular environment, we used fluo-3 as an alternative to fluo-3 AM. Treatment of fluo-3 in medium containing $CaCl_2$ as a source of calcium with both compounds showed no effect on

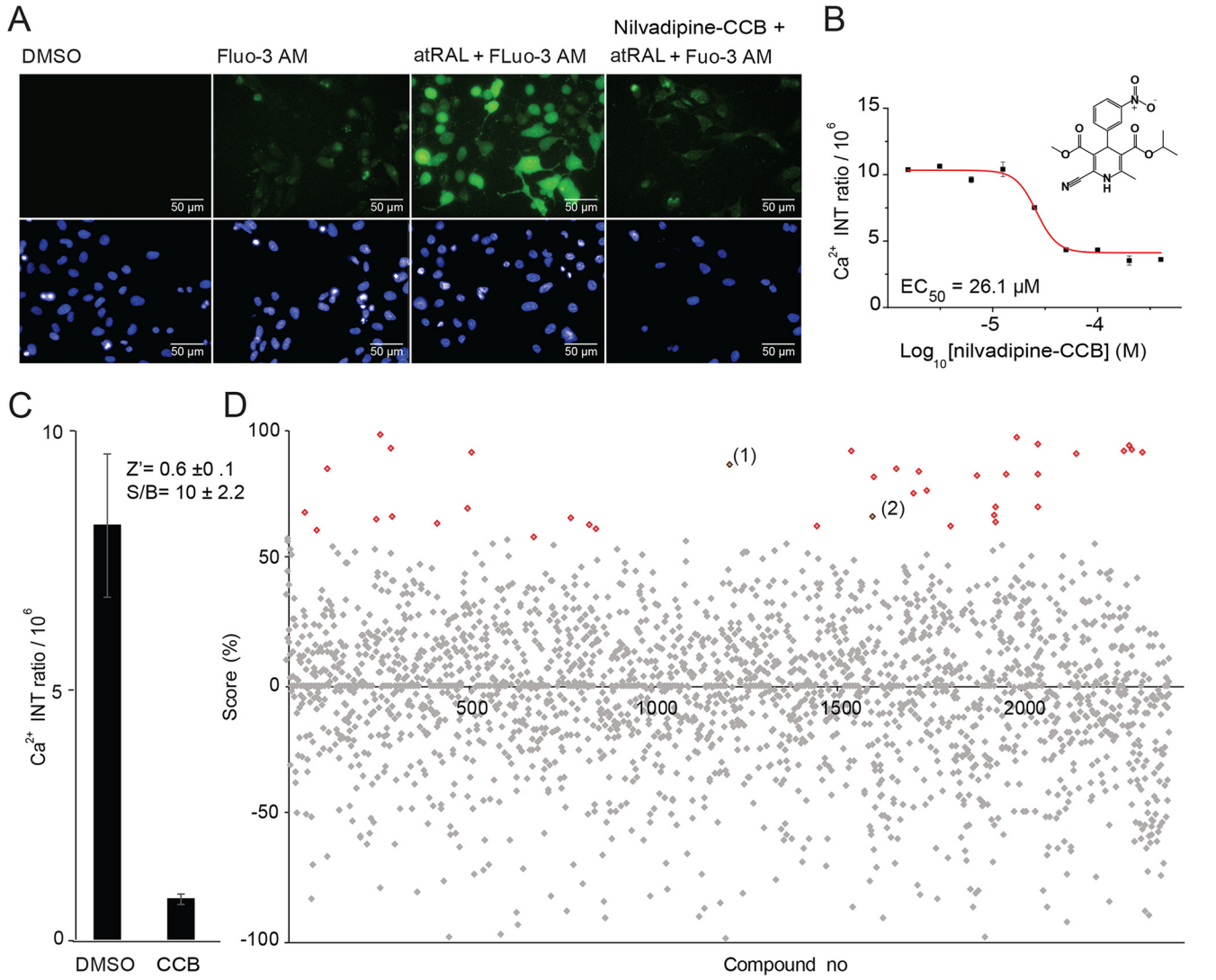

Figure 4. HTS calcium influx assay. *A*, high-content images of calcium intensity (*green*) controls: nontreated cells (DMSO), dye only–treated cells (fluo-3 AM), atRAL-treated cells, and drug (CCB)-pretreated cells. *B*, dose–response effect of nilvadipine (CCB) tested in 0.8–200 μM concentrations. *Error bars*, S.D. of triplicate readings. *C*, average fluorescence intensity quantification of U2OS cells exposed to atRAL with and without nilvadipine pretreatment. *Error bars*, S.D. of 16 replicate determinations. Shown are the HTS quality control parameters S/B ratio and *Z'* (*inset*). *D*, activity score plot of the 2,400-compound library screen. The screen identified 37 drugs (*red versus gray*) that block the rise in intracellular calcium due to atRAL exposure (activity score ≥60%). Cells exposed to atRAL were used to set the 0% score, and pre-nilvadipine-treated cells were used to establish the 100% score. Activity score = $(F_{comp} - F_{all})/(F_{all} - F_{CCB}) \times 100$ (where F_{comp} is fluorescent intensity of the tested compound, F_{all} is fluorescent intensity of atRAL only, and F_{CCB} is fluorescent intensity of CCB). Lead hits toremifene (**1**) and clomiphene (**2**) are indicated.

the calcium chelation property of fluo-3, suggesting that the *in vitro* activity of clomiphene and toremifene is due to intracellular signaling intervention (Fig. S4). Furthermore, we tested additional SERMs for their effects on calcium homeostasis after exposure to atRAL. The triphenylethylene parent compound tamoxifen showed a dose–response effect on decreasing the intracellular calcium concentration in the U2OS cells with an EC_{50} value of 17.9 μM, which corresponds to its retinal protection reported *in vivo*. However, the derivatives of tamoxifen, SAR-1 to SAR-4 had no effect on atRAL-induced calcium influx (Fig. S5), suggesting that the aminoethoxy side chain *para* substitution along with an isomerizable triphenyl ring are crucial for activity (Fig. 5, *B* and *C*). Tamoxifen metabolites in Fig. 5*D*, afimoxifene, endoxifen, and ospemifene (34), which exhibited more potent activities toward the estrogen receptor than tamoxifen, also demonstrated a dose-response protective effect against atRAL-induced calcium influx in a similar fashion as tamoxifen, with EC_{50} values of 16.8, 24.1, and 24.5 μM, respectively. The activity from these metabolites suggests that the presence of the tertiary amine and 4-position hydroxyl groups is not essential for activity. Two other family members of SERMs with different chemical cores, raloxifene and bazedoxifene, also showed dose-dependent effects on reducing calcium influx, with EC_{50} values of 17.7 and 4.31 μM, respectively (Fig. 5*E*), suggesting that the reduction of atRAL toxicity can be pharmacologically targeted through ERs, and it is not restricted by a single chemical scaffold.

A minor structural substitution of the raloxifene piperidine ring with the alkylated piperazine ring, Y 134 (35), dramatically abolished the dose-dependent effect of raloxifene (Fig. 5*F*). Wide structure–activity relationship studies on

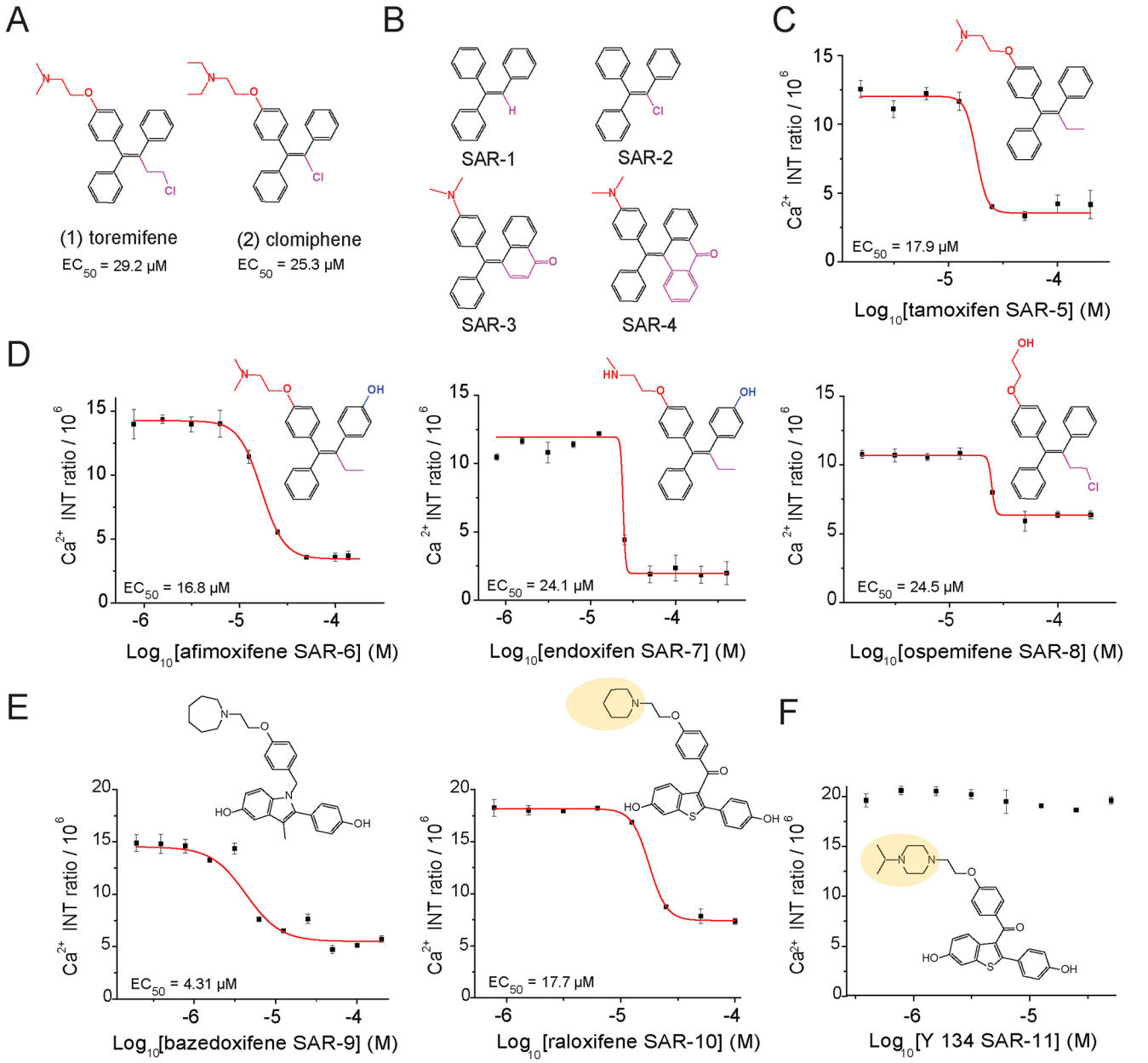

Figure 5. SERMs effect on intracellular calcium influx. *A*, chemical structures of identified SERM hits toremifene (**1**) and clomiphene (**2**) with the corresponding EC_{50} values. *B*, nonactive substructure modifications of triphenylethylene parent compounds (SAR-1 to SAR-4). *C*, dose–response effects and corresponding EC_{50} values of triphenylethylene parent compound tamoxifen on intracellular calcium signaling after atRAL treatment. *D*, tamoxifen parent metabolites afimoxifene, endoxifen, and ospemifene featuring structural changes in their aminoethoxy and aliphatic side chain (*red* and *purple*) along with a 4-position hydroxyl group (*blue*) showed a dose-dependent effect on intracellular calcium concentrations after exposure to atRAL. *E* and *F*, indole and benzothiophene scaffold SERMs: bazedoxifene, raloxifene, and Y 134 effects on intracellular calcium. Raloxifene and alkylated piperazine–substituted Y 134 demonstrated differing effects on intracellular calcium homeostasis in a dose-dependent manner. Concentrations ranged from 0.8 to 400 μM. *Error bars*, S.D. from experiments performed in triplicate.

benzothiophene-based SERMs have been performed (36–39), and the piperidine side chain of raloxifene is described to be essential for activity. Raloxifene derivative Y 134, containing a rigid piperazine side chain, can potentially impact the selectivity for ER subtype compared with those with a flexible chain (40). Selectivity for the ERα *versus* ERβ may account for the observed calcium activation-signaling phenomenon. To confirm the presence of target ERs in U2OS cells, we performed RT-PCR and were able to detect the transcript of three classical ERs: ERα (*Esr1*), ERβ (*Esr2*), and GPER30 (*Gper1*) (Fig. S6). Thus, in our *in vitro* study, we identified several effective candidates with $EC_{50} < 30$ μM in maintaining calcium homeostasis: clomiphene, toremifene, tamoxifen, afimoxifene, endoxifen, ospemifene, raloxifene, and bazedoxifene. Our preliminary *in vivo* test showed that all tested candidates displayed a variety of protective effects against light-induced photoreceptor degeneration in *Abca4*$^{-/-}$*Rdh8*$^{-/-}$ mice at a 40–100 mg/kg body weight dose range (data not shown). As a result, we decided to select raloxifene as our lead candidate along with its derivative Y 134 acting as an internal negative control *in vitro* and *in vivo*.

Protective effect of SERMs against bright light–induced retinal degeneration

The *Abca4*$^{-/-}$*Rdh8*$^{-/-}$ mouse model that is susceptible to bright light–induced retinal damage is a well-studied and widely used animal model for mechanistic and pharmacological studies of atRAL toxicity (5). Mice carrying a double knockout of *Rdh8*, which encodes an enzyme that reduces atRAL to atROL (41), and *Abca4*, which encodes a transporter that translocates atRAL from the inside to the outside of photoreceptor disc membranes (42, 43), rapidly accumulate atRAL. Then they manifest retinal pigmented epithelial (RPE) and photoreceptor dystrophy when they are exposed to a short period of bright light. To evaluate the protective effects of SERMs on atRAL-induced toxicity in acute light-induced photoreceptor degeneration *in vivo*, we treated *Abca4*$^{-/-}$*Rdh8*$^{-/-}$ mice with clomiphene (100 mg/kg), raloxifene (60 mg/kg), Y 134 (60 mg/kg), and vehicle control (DMSO). Mice at 6 weeks of age were given intraperitoneal (i.p.) injections 30 min prior to light exposure at 10,000 lux for 30 min, and the effect of treatment was assessed 7 days later (Fig. 6, *A* and *B*). Optical coherence tomography (OCT) scans revealed a significant reduction in the outer nuclear layer (ONL), demonstrating disrupted photoreceptor structures in DMSO and Y 134–treated mice, whereas clomiphene and raloxifene-treated mice exhibited a highly preserved retinal morphology like that of mice unexposed to bright light (Fig. 6, *C* and *D*). The efficacy of these treatments was further confirmed by scanning laser ophthalmoscopy (SLO) showing an increased number of autofluorescent spots likely due to infiltrating microglia and macrophages into the subretinal space in DMSO-treated (44) and Y 134–treated mice, whereas clomiphene and raloxifene-treated mice showed only a few autofluorescence spots in the superior region of the fundus (Fig. 6*E*). The efficacy profile of these SERMs in the retinal light damage model *in vivo* coincides with *in vitro* efficacies in the calcium influx assay.

Raloxifene treatment preserves retinal function

To determine the effects of raloxifene and Y 134 in rescuing visual function, we recorded the scotopic electroretinography (ERG) responses of *Abca4*$^{-/-}$*Rdh8*$^{-/-}$ mice preconditioned with raloxifene, Y 134, or DMSO at 10 days after the bright light challenge. Our results showed that raloxifene preserves both a- and b-wave ERG responses with similar amplitude and light sensitivity as unbleached mice. However, Y 134– and DMSO–treated mice showed substantially decreased ERG responses, indicating loss of photoreceptor function (Fig. 7). Our retinal morphological and electrophysiological analyses demonstrated that raloxifene but not Y 134 protects the retina from degeneration caused by light-induced accumulation of atRAL.

Cellular expression patterns of SERM targets

These neuroprotective effects of SERM compounds in the retina raise the question of exactly where and how they act. We addressed this using single-cell RNA (scRNA)-Seq data sets generated from adult mouse and human retinas (45). Somewhat surprisingly, we saw essentially undetectable expression of either Esr1, Esr2, or the plasma membrane estrogen receptor Gper1 in mice rod photoreceptors, whereas only Esr2 was detected in human rods (Fig. 8). In the retina, detectable levels of Esr1 were observed in horizontal cells in both mice and humans, whereas high levels of Gper1 were detected in endothelial cells in both species. This suggests either that SERM compounds protect photoreceptors from light damage through a cell nonautonomous mechanism or that they act on a yet unidentified target. Whereas estrogen-related receptors, particularly estrogen-related receptor β (Esrrb), are strongly and selectively expressed in rod photoreceptors (46) and have been shown to have neuroprotective function (47), these have been reported to be insensitive to raloxifene (48) and are unlikely targets for the observed effect.

Discussion

atRAL is a critical player in the pathogenesis of retinal degeneration through its association with photoreceptor cell degeneration (9, 49). In this study, we pharmacologically characterized the cytotoxicity of atRAL in cultured cells with various concentrations and incubation times. Our real-time measurements of calcium intensity revealed that atRAL rapidly induces calcium influx prior to cell death in a dose-dependent manner. We have shown that all visual cycle– essential retinals, including atRAL, 11-*cis*RAL, and 9-*cis*RAL, induce calcium influx that eventually causes cell apoptosis. Pharmacologically scavenging the aldehyde moiety of these vitamin A derivatives effectively abolished their cytotoxicity from disrupting calcium homeostasis, confirming that the aldehyde moiety is the cytotoxic source of atRAL. Herein, we developed a robust and sensitive image-based assay that detected changes in calcium homeostasis, using a calcium fluorescent indicator, fluo-3 AM, as a means of identifying compounds that can inhibit atRAL toxicity. Previous *in vitro* studies indicate that the concentration of atRAL rapidly released from 100% bleached opsin is roughly 3 mM (50). Assuming that a 1% bleach represents an exposure to bright sunlight that produces about 30 μM atRAL (51, 52), the concentration of atRAL used in our HTS assay was equivalent to that achievable in the retina under normal conditions. To ensure the highest sensitivity possible in our HTS assay, we carefully optimized our protocol and method of data analysis to minimize systemic errors and determine a stringent hit selection cutoff value with rigorous statistical power.

From a small-scale screen of 2,400 pharmacologically active compounds, we identified 12 hits that protect cells from atRAL-induced calcium influx, which included antimalarial and antipsychotic drugs. We identified two SERMs from these hits and examined multiple derivatives of SERMs *in vitro* and *in vivo*. Our medicinal chemistry analysis showed that the calcium-associated signal transduction of SERMs is not restricted to a single chemical scaffold triggering rapid rises in intracellular calcium. Previous studies demonstrated that plasma membrane–associated ERs respond to estrogen administration with cAMP generation and calcium changes (53). mER signaling has been reported to mediate calcium influx via the L-type calcium channels activated by the Src/extracellular signal–regulated kinase/cAMP signaling cascade that is involved in the rapid intracellular calcium responses to estrogen (22). atRAL is known to activate the phospholipase C/inositol trisphosphate-mediated calcium signaling via modulating

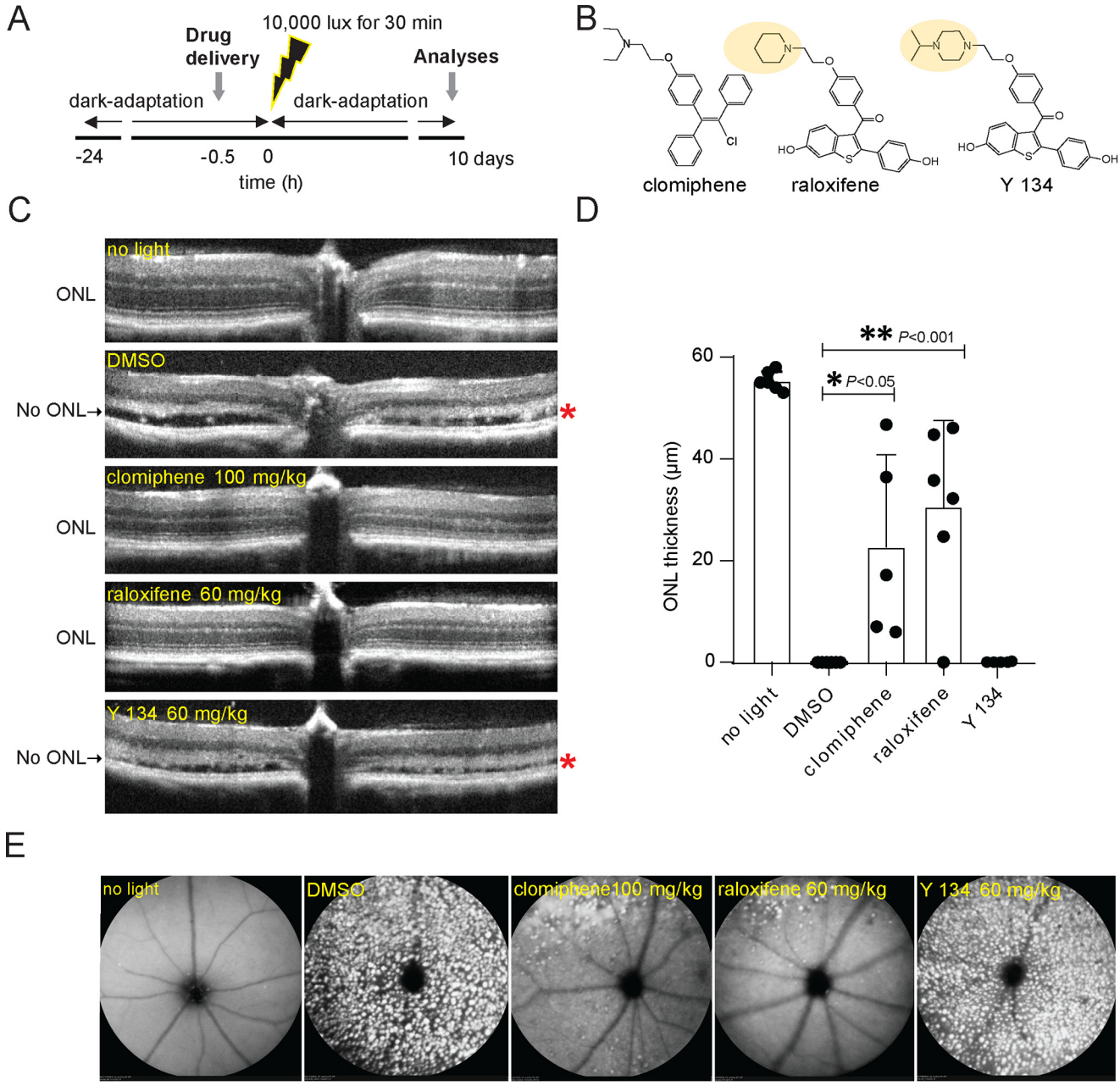

Figure 6. Protective effects of SERMs against light-induced retinal degeneration in *Abca4*$^{-/-}$*Rdh8*$^{-/-}$ mice. *A*, *schematic* of the experimental protocol. *Abca4*$^{-/-}$*Rdh8*$^{-/-}$ mice were dark-adapted 24 h prior to clomiphene, raloxifene, Y 134, or DMSO administration to 6-week-old male and female mice. Mice were intraperitoneally injected 30 min before exposure to bright light at 10,000 lux for 30 min. Mice were kept in the dark for 7 days before OCT and SLO were performed. *B*, chemical structures of clomiphene, raloxifene, and Y 134. *C*, representative retinal OCT images obtained 7 days after *Abca4*$^{-/-}$*Rdh8*$^{-/-}$ mice were either unexposed to bright light (no light) or exposed to bright light after pretreatment with DMSO or the indicated compounds (clomiphene, raloxifene, and Y 134) at the doses of 100, 60, and 60 mg/kg, respectively. *, completely damaged ONL with severe retinal detachment in DMSO– and Y 134–treated mice. *D*, quantification of the ONL thickness was determined from OCT images from 5–6 mice 7 days after light exposure. Changes in the ONL thickness observed after treatment with clomiphene and raloxifene compounds compared with the DMSO– and Y 134–treated group were statistically significant ($p < 0.001$ and $p < 0.05$). *E*, representative SLO images show the retinas of *Abca4*$^{-/-}$*Rdh8*$^{-/-}$ mice unexposed to bright light or exposed to light after the indicated pretreatment. Mice unexposed to bright light or exposed to bright light after pretreatment with clomiphene and raloxifene exhibited fewer autofluorescent spots, indicating less damage of the retinas. *Error bars*, S.D. of five animal replicas.

the G_q and G_s cascades (6). Thus, antagonizing ER activity may restrain calcium influx directly or indirectly against atRAL-mediated pathways. Expression of ERs in the retina already has been shown by others (54) and was again confirmed in our RT-PCR and scRNA-Seq analysis. However, it is important to mention that the low expression level of ERs in both U2OS cells and mouse retina are not detectable on Western blotting to confirm the presence of ERs in a protein level. For this reason, we performed RT-PCR to support the presence of ER transcripts in U2OS cells and included scRNA-Seq analysis. Tamoxifen, a member of the SERMs, was previously reported to protect the retina from light damage *in vivo* (33). Our *in vivo* results further validated that other SERMs, such as clomiphene and raloxifene, effectively protect the retina from light-induced atRAL toxicity, and the efficacies of tested SERMs are consistent with their *in vitro* activities in blocking atRAL-induced calcium flux.

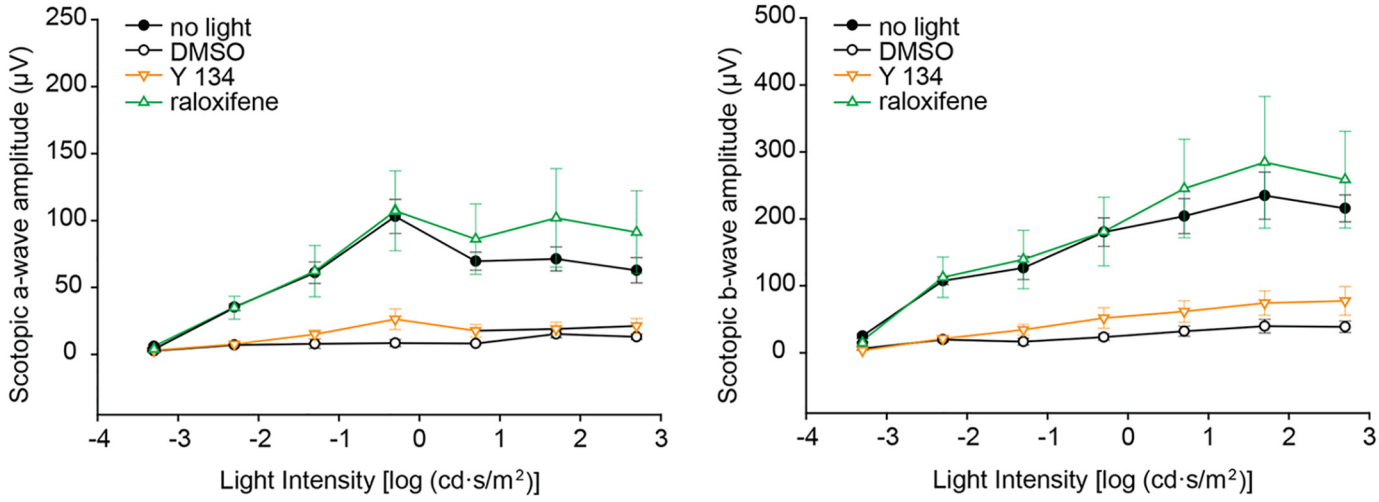

Figure 7. Retinal function in *Abca4*$^{-/-}$*Rdh8*$^{-/-}$ mice is substantially preserved by SERM raloxifene. ERG recordings of scotopic a-wave (*left*) and b-wave (*right*) were plotted to evaluate the retinal function of drug-treated *Abca4*$^{-/-}$*Rdh8*$^{-/-}$ mice 10 days after light-induced damage. Both a-wave amplitude, which reflects the response from photoreceptors, and b-wave amplitude, which reflects the response of downstream bipolar cells, were significantly higher in the raloxifene-treated group as compared with the DMSO and Y 134–treated groups ($p < 0.05$). Compared with the unbleached control group (no light), the raloxifene-treated group showed no significant difference in a- and b-wave amplitudes, suggesting that raloxifene provides nearly full protection of the retina against the light-induced damage. $n = 4–5$. Data are shown as means ± S.E. (*error bars*).

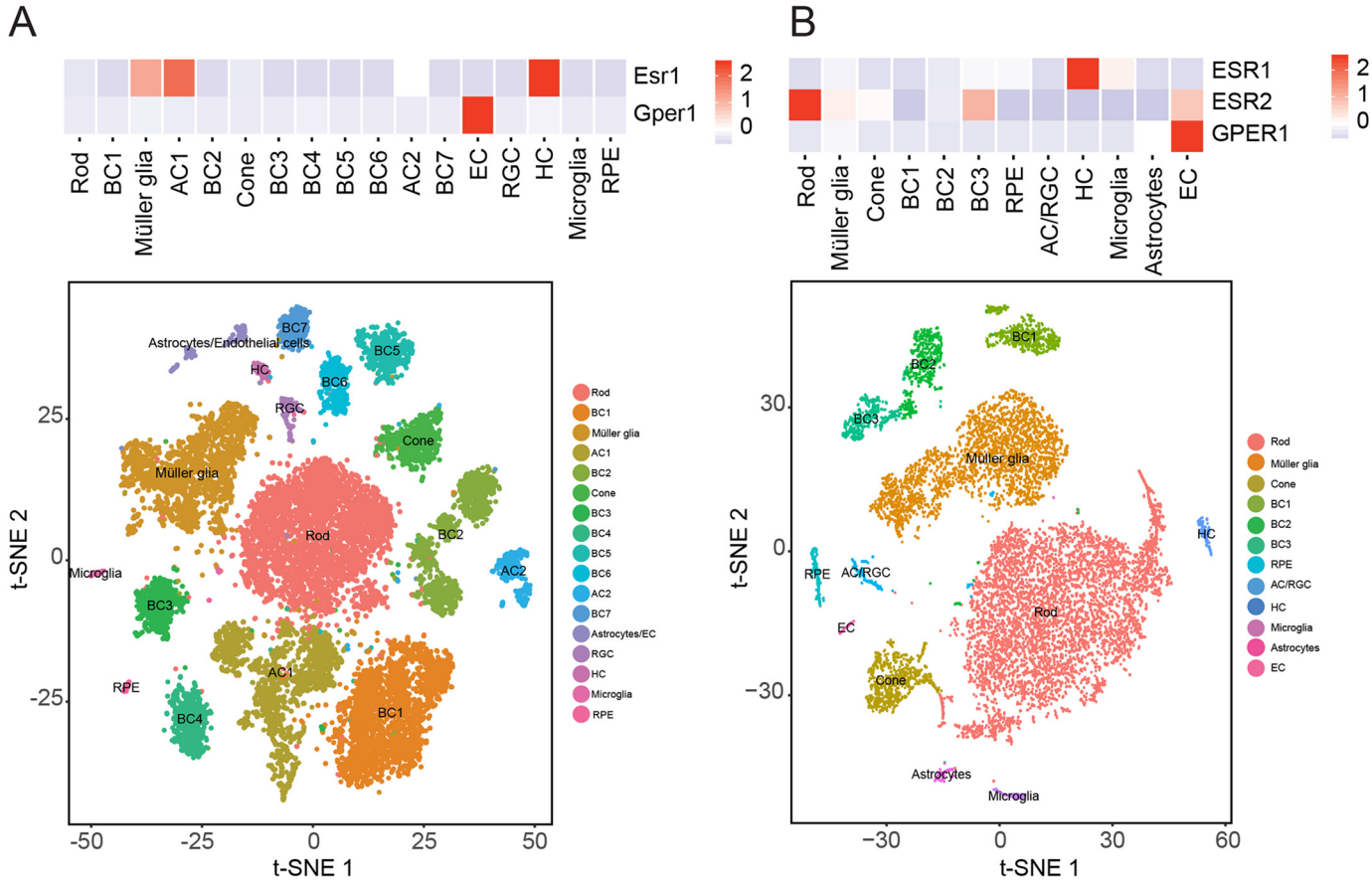

Figure 8. scRNA-Seq analysis of ER expression in mouse and human retinas. *Heat maps* show the correlation between the expressions of ER genes in different cell clusters from adult mouse (*A*) and human whole retina (*B*) at the single-cell level. *AC*, amacrine cells; *BC*, bipolar cells; *HC*, horizontal cells; *RGC*, retinal ganglion cells; *EC*, endothelial cells. The *color intensity* in the *heat map* is based on the expression levels of ER genes in the retina.

To our knowledge, this is the first study demonstrating that the retinal protective effect of the benzothiophene family of SERMs may be attributed to the inhibition of atRAL-induced calcium elevation in the retina. In this examination, we developed a model that pharmacologically targeting mER inhibits atRAL-induced calcium elevation that protects the retina from light-induced toxicity. We previously showed that pharmacologically targeting G protein–coupled receptors activating the G_i cascade or inactivating the G_q and G_s cascades effectively protects retina from light damage as well (55). In this study, we

revealed that mER is a valid and novel target for treating retinal degeneration associated with atRAL toxicity, which adds to our current system pharmacology inventory for synergistic treatments of retinal degenerative diseases. However, the absence of expression in photoreceptors of the known components of mER (Esr1, Esr2, and Gper1) suggests that the neuroprotective effects of these compounds on photoreceptors may reflect either non-cell-autonomous effects of SERMs or their action on currently unknown molecular targets. The consistency of our *in vitro* and *in vivo* results validated that our HTS assay is a highly unbiased, robust, and sensitive assay for identifying potent drug candidates and novel molecular targets protecting the retina from atRAL toxicity via large-scale small-molecule libraries or RNAi screens.

Experimental procedures

Chemicals

atRAL, atROL, 9-*cis*RAL, nilvadipine, triflupromazine, toremifene, micanazole, ebselen, clomiphene, gambogic acid, plumbagin, zinc pyrithione, sanguinarine, mefloquine, sulconazole, hexylresorcinol, triphenylethylene (**1**), 1-chloro-triphenylethylene (**2**), 10-(4-(dimethylamino)-α-phenylbenzylidene)-9-anthrone (**3**), 4-(4-(dimethylamino)-α-phenylbenzylidene)-1(4H)-naphthalenone (**4**), tamoxifen, afimoxifene, ospemifene, and endoxifen were all purchased from Sigma-Aldrich. A2E was synthesized as described previously (56), and 11-*cis*RAL was isolated as described previously (57). Fluo-3 AM was purchased from AAT Bioquest Inc. (Sunnyvale, CA). Noncellular fluo-3 was obtained from Thermo Fisher Scientific (Waltham, MA). MB-001, MB-002, and emixustat were synthesized as described previously (26, 58). The Spectrum Collection containing 2,400 pharmacologically active compounds was purchased from MicroScource (Gaylordsville, CT). Raloxifene, bazedoxifene, and Y 134 were obtained from Tocris Bioscience (Bristol, UK).

Nuclease morphology measurements in U2OS cells after atRAL treatment

On day 1, U2OS cells were detached from their tissue culture flasks with 0.25% trypsin (Thermo Fisher Scientific) and suspended in DMEM, high-glucose medium containing 10% fetal bovine serum and 1% penicillin-streptomycin (10,000 units/ml) (Thermo Fisher Scientific). Cells were counted and then diluted to 20×10^4 cells/ml. The cell diluent was dispensed into a black 384-ViewPlate with an optically clear bottom (PerkinElmer Life Sciences) at 20 μl/well. On day 2, 5 μl of atRAL (Sigma-Aldrich) was added to each well to achieve a final concentration of 90, 45, 30, 15, or 7.5 μM in triplicates. Hoechst 33342 (Sigma-Aldrich) nucleic acid stain was used as a cell-permeant nuclear counterstain that emits blue fluorescence when bound to dsDNA. After an incubation for 15 min at 3 μM final concentration, fluorescent intensity of nuclease morphology was detected with an Operetta high-content imaging system (PerkinElmer Life Sciences) using bright-field and UV light source along with an analysis implemented by Harmony® high-content imaging and analysis software (59). Cells were subsequently cultured and monitored for 3 days. Nuclease morphology was color-coded as follows: *red*, dead cells, nuclear area < 200 pixels^2; *green*, live cells, nuclear area > 200 pixels^2.

Cell viability assay after atRAL exposure

U2OS cells were detached from the tissue culture flask with 0.25% trypsin (Thermo Fisher Scientific) and suspended in DMEM, high-glucose medium containing 10% fetal bovine serum and 1% penicillin-streptomycin (10,000 units/ml) (Thermo Fisher Scientific). Cells were counted with a hemocytometer and then diluted to about 3×10^4 cells/ml. The cell diluent was dispensed into a black 384-ViewPlate, with an optically clear bottom (PerkinElmer Life Sciences) at 40 μl/well using an EL406 plate dispenser (BioTek, Winooski, VT). Column 1 contained only medium to serve as a control with no ATP. The next day, 5 μl of atRAL (Sigma-Aldrich) was added to each well to achieve a final concentration of 60, 30, or 15 μM. Cells were cultured at 37 °C with 5% CO_2 for 1 h or overnight. After culturing, cells were treated with 25 μl of CellTiter-Glo reagent (Promega, Madison, WI) and incubated at room temperature for 1 h to stabilize the luminescent signal (60, 61). Luminescence was recorded on a SpectraMax L plate reader (Molecular Devices, San Jose, CA).

Intracellular calcium influx assessment after atRAL exposure

On day 1, cells were seeded in 384-well plates as described above. On day 2, cells were treated with 10 μl of 180, 120, and 90 μM atRAL (Sigma-Aldrich) in culture medium to achieve a 30, 20, and 15 μM final concentration and incubated for 15 min, followed by treatment with 10 μl of cell-permeable fluo-3 AM (AAT Bioquest, Inc.), to achieve a 3 μM final concentration. Subsequently, plates were incubated at 37 °C with 5% CO_2 for 30 min, using an EL406 plate washer/dispenser (BioTek), followed by three washes with 1.05 mM KH_2PO_4, 155.1 mM NaCl, and 2.96 mM Na_2HPO_4-$7H_2O$, pH 7.4 (PBS). Cells were then incubated with 30 μl of 10 μM Hoechst 33342 (Sigma-Aldrich) in PBS to achieve a 3 μM final concentration. After incubation for 3 h, the fluorescent intensity of cells was detected with an Operetta high-content imaging system (PerkinElmer Life Sciences) (8–10, 62). U2OS cells were treated with 10 μl of 180 μM 11-*cis*RAL, 9-*cis*RAL, atRAL, atROL, or A2E similarly as atRAL in culture medium to achieve a 30 μM final concentration for 15 min as described above. After incubation for 3 h, fluorescent intensity of cells was imaged as described above. The assessment was performed in various cell types, including U2OS, NIH3T3, ARPE19, Chinese hamster ovary, HEK293, and MCF-7 cells.

atRAL quenchers

U2OS cells were cultured in 384-well plates (1,050 cells/well), at 37 °C overnight and then further incubated with MB-001, MB-002, and emixustat in a dose-dependent manner with concentrations ranging from 0.8 to 200 μM in triplicates. The following day, the cells were treated with 30 μM atRAL (Sigma-Aldrich) for 15 min, followed by a 30-min incubation with 3 μM cell-permeable fluorescent calcium indicator fluo-3 AM (AAT Bioquest, Inc.). Cells were then washed three times with PBS and then incubated with 3 μM Hoechst 33342 (Sigma-Aldrich) for another 3 h at 37 °C with 5% CO_2. Fluorescence measurements using an Operetta high-content imaging system (PerkinElmer Life Sciences) were performed as described previously (11).

HTS calcium influx assay

On day 1, cells were detached from the tissue culture flask with 0.05% trypsin (Thermo Fisher Scientific) and suspended in DMEM, high-glucose medium containing 10% fetal bovine serum and 1% penicillin-streptomycin (10,000 units/ml) (Thermo Fisher Scientific). Cells were diluted to 26,250 cells/ml. The cell diluent was dispensed into a black ViewPlate-384 plate, with an optically clear bottom (PerkinElmer Life Sciences) at 40 μl/well using an EL406 plate dispenser (BioTek) and cultured at 37 °C in 5% CO_2 at 90% humidity. On day 2, columns 3–22 of the 384-well plates were treated with a 2,400 pharmacologically active compound library (MicroScource). Each well was treated with 44 nl of 10 mM drug stock in DMSO using a JANUS workstation (PerkinElmer Life Sciences), calibration of the 384 pins using serial dilutions of known concentration of rhodamine and measuring the corresponding fluorescence was determined, and concentrations were adjusted accordingly to achieve an 11 μM final concentration. Columns 1, 2, and 23 were used as DMSO-treated controls (column 1, DMSO only; column 2, DMSO and fluo-3 AM; column 23, DMSO, fluo-3 AM, and atRAL in 16 replicates each). Column 24 was used as a calcium channel blocker control in 16 replicates. Parallel to the library screen, columns 1, 2, and 23 were treated with 0.01% DMSO, and column 24 was treated with a 50 μM final concentration of nilvadipine (CCB) (Sigma-Aldrich). On day 3, column 1 was left untreated, and columns 3–24 were incubated for 15 min with 30 μM atRAL. Subsequently, columns 2–24 were treated with 3 μM cell-permeable calcium indicator fluo-3 AM (AAT Bioquest, Inc.) and incubation for 30 min. Cells were then washed with PBS and treated with 3 μM Hoechst 33342 (Sigma-Aldrich) using the EL406 plate washer/dispenser (BioTek). After a 3-h incubation at 37 °C with 5% CO_2, the fluorescence intensity of cells using appropriate wavelength settings (excitation/emission at 506/526 nm) was detected with an Operetta high-content imaging system (PerkinElmer Life Sciences) along with an analysis implemented by Harmony® high-content imaging and analysis software. The quality control parameters, the signal/background ratio (S/B ratio), and Z' values were calculated as follows: S/B ratio = $\text{mean}_{100\%\ \text{control}}/\text{mean}_{0\%\ \text{control}}$; $Z' = 1–3\times (\text{S.D.}_{0\%\ \text{control}} + \text{S.D.}_{100\%\ \text{control}})/(\text{mean}_{100\%\ \text{control}} - \text{mean}_{0\%\ \text{control}})$ (63); 100% control, atRAL-treated cells; and 0% control, CCB treated cells prior to atRAL exposure. The quality control parameters demonstrated S/B ratios greater than 10 ± 2.2 and Z' greater than 0.6 ± 0.1. All hit compounds were retested in triplicates with concentrations ranging from 0.2 to 400 μM.

Dose-dependent assay of calcium influx for hit validation and medicinal chemistry

Our developed HTS image-based assay was used to evaluate the effects of nilvadipine, triflupromazine, toremifene, micanazole, ebselen, clomiphene, gambogic acid, plumbagin, zinc pyrithione, sanguinarine, mefloquine, sulconazole, hexylresorcinol, triphenylethylene (**1**), 1-chlorotriphenylethylene (**2**), 10-(4-(dimethylamino)-α-phenylbenzylidene)-9-anthrone (**3**), 4-(4-(dimethylamino)- α-phenylbenzylidene)-1(4H)-naphthalenone (**4**), tamoxifen, afimoxifene, ospemifene, endoxifen, MB-001, MB-002, emixustat, raloxifene, bazedoxifene, and Y 134 on intracellular calcium influx, associated with atRAL treatment in a dose-dependent manner with the concentrations ranging from 0.2 to 400 μM in triplicates using an automated JANUS work station (PerkinElmer Life Sciences).

Counterscreen measuring the noncellular fluo-3 effect on identified hits

Fluo-3, pentapotassium salt (Thermo Fisher Scientific) was used to image the spatial dynamics of calcium signaling with identified HTS hits with concentrations ranging from 0.8 to 200 μM in triplicates. DMEM, high-glucose medium was dispensed into a black ViewPlate-384 plate, with an optically clear bottom (PerkinElmer Life Sciences) at 40 μl/well using an EL406 plate dispenser (BioTek). Columns 3–22 of the 384-well plates were treated with all identified hits in a dose-dependent manner using a JANUS workstation (PerkinElmer Life Sciences). The following day, columns 2–23 were incubated for 15 min with 30 μM atRAL, followed by fluo-3 treatment for 30 min. After a 3-h incubation, the fluorescent intensity was measured using an EnSpire Multimode Plate Reader (PerkinElmer Life Sciences) with excitation and emission at 506- and 526-nm wavelengths, respectively.

Animals and treatments

Abca4$^{-/-}$*Rdh8*$^{-/-}$ double knockout mice (5) were used to evaluate the protective effect of SERMs in light-induced retinal degeneration. Clomiphene, raloxifene, and Y 134 were dissolved in DMSO and administered to mice by i.p. injection at 100, 60, and 60 mg/kg body weight, respectively. Both male and female mice were used in all experiments, and no significant sexual differences were seen in responses to treatments. All mice were housed in the University Laboratory Animal Resources facilities at the University of California (Irvine, CA) and maintained in a 12-h light (~300 lux)/dark cycle. Adaptations in the dark were performed under dim red light. All experiments were conducted according to protocols approved by a local institutional animal care and use committee (approval no. AUP-18-124) at the University of California (Irvine, CA).

Inducing light damage

Abca4$^{-/-}$*Rdh8*$^{-/-}$ double knockout mice were dark-adapted for 24 h before exposure to bright light. Retinal degeneration was initiated by exposing dark-adapted mice to 10,000 lux of diffuse white fluorescent light (150-watt spiral lamp) for 30 min as described previously (12). Before light exposure, pupils of mice were dilated with 1% tropicamide (Akorn, Inc., Lake Forest, IL). After exposure, animals were kept in the dark until evaluation. Clomiphene, raloxifene, Y 134, or DMSO was administered intraperitoneally 30 min before exposure to bright light. Effects of clomiphene, raloxifene, Y 134, and DMSO were tested at 100 to 60 mg/kg of body weight. Each injection volume was 50 μl. Retinal morphology and function were analyzed *in vivo* by spectral domain optical coherence tomography (SD-OCT), SLO, and ERG.

SLO imaging and SD-OCT

SLO (HRAII, Heidelberg Engineering) and SD-OCT (Envisu™ C-Class SDOIS) were employed for *in vivo* imaging of mouse

retinas as implemented in previous publications (12, 64). Briefly, mice were anesthetized by i.p. injection of ketamine (20 mg/ml) and xylazine (1.8 mg/ml) at a dose of 100 μl/20 g body weight. Pupils of *Abca4*$^{-/-}$*Rdh8*$^{-/-}$ double knockout mice were dilated with 1% tropicamide. The accumulation of autofluorescent spots (particles) can be observed in the retina by SLO imaging in the autofluorescence mode (65). Twenty OCT images acquired in the B-scan mode were averaged to five at 0° (showing temporal and nasal retina) and 90° (showing superior and inferior retina) and saved for ONL thickness measurements. To evaluate changes in the retinas of mice exposed to bright light, the ONL thickness was measured 500 μm from the optic nerve head (5–6 mice/group).

ERG

The ERG responses were measured 10 days after light-induced damage in raloxifene–, Y 134–, and DMSO–treated groups along with the unbleached group as described previously (66). Each group consisted of 4–5 *Abca4*$^{-/-}$*Rdh8*$^{-/-}$ mice 6 weeks of age. Prior to recording, mice were dark-adapted for 24 h. Under dim red light, mice were anesthetized by i.p. injection of ketamine (20 mg/ml) and xylazine (1.8 mg/ml) at a dose of 100 μl/20 g body weight. Pupils were dilated with 1% tropicamide, and 2.5% hypromellose was applied to keep the corneas hydrated. Contact lens electrodes were placed onto the corneas, and the reference and ground electrode needles were placed on the forehead and tail, respectively. The a-wave and b-wave responses were measured, followed by a light stimulus of different flash intensities (−3.3 to 2.7 log candelas·s/m^2). For each intensity, 3–20 recordings were taken and averaged with the resting intervals for recovery from photobleaching effects. All ERGs were recorded with the Celeris ophthalmic electrophysiology system (Diagnosys LLC, Lowell, MA) and analyzed with Espion version 6 software (Diagnosys LLC).

RT-PCR, gel electrophoresis, and sequencing for detection of estrogen receptors

Total RNA from MCF-7 and U2OS cells and mouse retinas were isolated by using the RNeasy Plus kit (Qiagen, Hilden, Germany) following the manufacturer's instructions. Total mouse brain RNA was purchased from Takara (Kusatsu, Japan). One μg of purified RNA from each sample was reverse-transcribed to cDNA using a High-Capacity RNA-to-cDNA Kit (Applied Biosystems, Foster City, CA), and the cDNA was used for performing PCRs using the primers in Table S1. PCRs were set up using PowerUp SYBR Green Master Mix (Thermo Fisher Scientific) following the manufacturer's instructions. The cycling protocol used was 95 °C for 1 s, 60 °C for 30 s for 40 cycles. The final PCR products were separated in 1.5% agarose gel stained with SYBR Safe DNA gel stain (Invitrogen) and visualized using an Odyssey Fc imaging system (LI-COR, Lincoln, NE). The remaining volume of PCR products was purified using a QIAquick PCR Purification Kit (Qiagen) and was subjected to Sanger sequencing to ensure the amplification from correct target.

scRNA-Seq

For tissue dissection and cell dissociation, a human globe from an 86-year-old Caucasian female who died of a myocardial infarction and had no known ocular disease other than cataracts was obtained from the Alabama Eye Bank (Birmingham, AL) and processed within 3.3 h after death. The study was approved by the Johns Hopkins Institutional Review Board. The neural retina and RPE/choroid were dissected from the globe in ice-cold PBS. First, a circular incision was made on the sclera, behind the limbus, to remove the anterior parts, lens, and vitreous body. The neural retina was then peeled off from the eyecup and dissociated using the Papain Dissociation System (Worthington) following the manufacturer's instructions. RPE cells were dissociated from the eyecup by incubating with 2 ml of 0.05% EDTA (Thermo Fisher Scientific) for 20 min at 37 °C. Dissociated cells were resuspended in ice-cold PBS, 0.04% BSA, and 0.5 units/μl RNase inhibitors.

CD1 mice between 7 and 9 weeks of age were purchased from Charles River Laboratories (Wilmington, MA). All experimental procedures were pre-approved by the institutional animal care and use committee of the Johns Hopkins University School of Medicine. Mice were euthanized, and eye globes were removed and incubated in ice-cold PBS. Retinas were dissected, and cells were dissociated using the Papain Dissociation System. In total, four biological replicates were used for the mouse scRNA study. Each replicate contained four retinas from each of two male and two female mice. Dissociated cells were resuspended in ice-cold PBS, 0.04% BSA, and 0.5 units/μl RNase inhibitors. Cell count and viability were assessed by trypan blue staining.

For scRNA-Seq, dissociated cells (~10,000) were loaded into a 10× Genomics Chromium Single Cell system (10× Genomics, CA) using v2 chemistry following the manufacturer's instructions (67). Libraries were pooled and sequenced on Illumina NextSeq with ~200 million reads per library. Sequencing results were processed through the Cell Ranger 2.1.1 pipeline (10× Genomics) with default parameters. Seurat version 2.3.1 (68) was used to perform downstream analysis following the standard pipeline using cells with more than 200 genes and 1,000 UMI counts, resulting in 16,659 mouse cells and 14,286 human cells. Samples were aggregated, and cell clusters were annotated based on previous literature (45). A *t*-distributed stochastic neighbor-embedding dimension reduction was performed on the top principal components learned from high variance genes. Mclust version 5.4 was used to cluster cells in the *t*-distributed stochastic neighbor-embedding space, at which point cell type identity of clusters was assigned based on the expression of known marker genes for either retinal or nonretinal tissue.

Statistical analyses

HTS image analysis was performed with Harmony® high-content image analysis software, and average intensities of the FITC channel were exported in spreadsheet software. Z'-Factor was calculated for each parameter to evaluate the assay quality as described above. A Z'-factor higher than 0 indicates a moderate assay sufficient for a high-content screen, and a Z'

factor between 0.5 and 1 suggests an outstanding assay required for a high-throughput screen (69). Controls used in the screen included 16 replicates, whereas compounds were tested in triplicate at 6–10 concentrations for dose dependence evaluation as means ± S.D.

For animal studies, results were collected from at least four mice from each experimental group determined by a power analysis to ensure sufficient statistical power with $\alpha \leq 0.05$ (type I error) and $1 - \beta \geq 0.90$ (power) (70). Statistical analyses were performed with analysis of variance on ranks with Dunn's post hoc test. Data are presented as means ± S.E. $p \leq 0.05$ is considered statistically significant.

Author contributions—T. G. participated in conceptualization, obtaining resources, data curation, formal analysis, investigation, methodology, writing-original draft, project administration, and writing-review and editing. S. S. participated in research design, conducted experiments, contributed new reagents or analytical tools, performed data analysis, and contributed to manuscript writing. T. H., J. T. H., and Z. D. participated in research design, conducted experiments, contributed new reagents or analytical tools, and performed data analysis. X. M. conducted experiments. Y. C. and S. B. participated in research design, contributed new reagents or analytical tools, and contributed to manuscript writing. K. P. participated in research design and contributed to manuscript writing.

Acknowledgments—We thank members of the Case Western Reserve University School of Medicine Small Molecule Drug Development Core facilities for guidance through the development of the HTS assays.

References

1. Aboul-Enein, H. Y., and Ali, I. (2002) Comparative study of the enantiomeric resolution of chiral antifungal drugs econazole, miconazole and sulconazole by HPLC on various cellulose chiral columns in normal phase mode. *J. Pharm. Biomed. Anal.* **27,** 441–446 CrossRef Medline
2. von Lintig, J., Kiser, P. D., Golczak, M., and Palczewski, K. (2010) The biochemical and structural basis for *trans*-to-*cis* isomerization of retinoids in the chemistry of vision. *Trends Biochem. Sci.* **35,** 400–410 CrossRef Medline
3. McBee, J. K., Palczewski, K., Baehr, W., and Pepperberg, D. R. (2001) Confronting complexity: the interlink of phototransduction and retinoid metabolism in the vertebrate retina. *Prog. Retin. Eye Res.* **20,** 469–529 CrossRef Medline
4. Kiser, P. D., Golczak, M., Maeda, A., and Palczewski, K. (2012) Key enzymes of the retinoid (visual) cycle in vertebrate retina. *Biochim. Biophys. Acta* **1821,** 137–151 CrossRef Medline
5. Maeda, A., Maeda, T., Golczak, M., and Palczewski, K. (2008) Retinopathy in mice induced by disrupted all-*trans*-retinal clearance. *J. Biol. Chem.* **283,** 26684–26693 CrossRef Medline
6. Chen, Y., Okano, K., Maeda, T., Chauhan, V., Golczak, M., Maeda, A., and Palczewski, K. (2012) Mechanism of all-*trans*-retinal toxicity with implications for Stargardt disease and age-related macular degeneration. *J. Biol. Chem.* **287,** 5059–5069 CrossRef Medline
7. Quazi, F., and Molday, R. S. (2014) ATP-binding cassette transporter ABCA4 and chemical isomerization protect photoreceptor cells from the toxic accumulation of excess 11-*cis*-retinal. *Proc. Natl. Acad. Sci. U.S.A.* **111,** 5024–5029 CrossRef Medline
8. Holownia, A., Ledig, M., Braszko, J. J., and Ménez, J. F. (1999) Acetaldehyde cytotoxicity in cultured rat astrocytes. *Brain Res.* **833,** 202–208 CrossRef Medline
9. Maeda, A., Maeda, T., Golczak, M., Chou, S., Desai, A., Hoppel, C. L., Matsuyama, S., and Palczewski, K. (2009) Involvement of all-*trans*-retinal in acute light-induced retinopathy of mice. *J. Biol. Chem.* **284,** 15173–15183 CrossRef Medline
10. Kruman, I. I., and Mattson, M. P. (1999) Pivotal role of mitochondrial calcium uptake in neural cell apoptosis and necrosis. *J. Neurochem.* **72,** 529–540 CrossRef Medline
11. Maeda, A., Golczak, M., Chen, Y., Okano, K., Kohno, H., Shiose, S., Ishikawa, K., Harte, W., Palczewska, G., Maeda, T., and Palczewski, K. (2011) Primary amines protect against retinal degeneration in mouse models of retinopathies. *Nat. Chem. Biol.* **8,** 170–178 CrossRef Medline
12. Chen, Y., Palczewska, G., Mustafi, D., Golczak, M., Dong, Z., Sawada, O., Maeda, T., Maeda, A., and Palczewski, K. (2013) Systems pharmacology identifies drug targets for Stargardt disease-associated retinal degeneration. *J. Clin. Invest.* **123,** 5119–5134 CrossRef Medline
13. Clark, J. H., and Markaverich, B. M. (1981) The agonistic-antagonistic properties of clomiphene: a review. *Pharmacol. Ther.* **15,** 467–519 CrossRef Medline
14. Greenblatt, R. B. (1961) Chemical induction of ovulation. *Fertil. Steril.* **12,** 402–404 CrossRef Medline
15. Dickey, R. P., and Holtkamp, D. E. (1996) Development, pharmacology and clinical experience with clomiphene citrate. *Hum. Reprod. Update* **2,** 483–506 CrossRef Medline
16. Holli, K., Valavaara, R., Blanco, G., Kataja, V., Hietanen, P., Flander, M., Pukkala, E., and Joensuu, H. (2000) Safety and efficacy results of a randomized trial comparing adjuvant toremifene and tamoxifen in postmenopausal patients with node-positive breast cancer. Finnish Breast Cancer Group. *J. Clin. Oncol.* **18,** 3487–3494 CrossRef Medline
17. Sawaki, M., Wada, M., Sato, Y., Mizuno, Y., Kobayashi, H., Yokoi, K., Yoshihara, M., Kamei, K., Ohno, M., and Imai, T. (2012) High-dose toremifene as first-line treatment of metastatic breast cancer resistant to adjuvant aromatase inhibitor: a multicenter phase II study. *Oncol. Lett.* **3,** 61–65 CrossRef Medline
18. Maximov, P. Y., Lee, T. M., and Jordan, V. C. (2013) The discovery and development of selective estrogen receptor modulators (SERMs) for clinical practice. *Curr. Clin. Pharmacol.* **8,** 135–155 CrossRef Medline
19. Early Breast Cancer Trialists' Collaborative Group (EBCTCG), Davies, C., Godwin, J., Gray, R., Clarke, M., Cutter, D., Darby, S., McGale, P., Pan, H. C., Taylor, C., Wang, Y. C., Dowsett, M., Ingle, J., and Peto, R. (2011) Relevance of breast cancer hormone receptors and other factors to the efficacy of adjuvant tamoxifen: patient-level meta-analysis of randomised trials. *Lancet* **378,** 771–784 CrossRef Medline
20. Ettinger, B., Black, D. M., Mitlak, B. H., Knickerbocker, R. K., Nickelsen, T., Genant, H. K., Christiansen, C., Delmas, P. D., Zanchetta, J. R., Stakkestad, J., Glüer, C. C., Krueger, K., Cohen, F. J., Eckert, S., Ensrud, K. E., *et al.* (1999) Reduction of vertebral fracture risk in postmenopausal women with osteoporosis treated with raloxifene: results from a 3-year randomized clinical trial: Multiple Outcomes of Raloxifene Evaluation (MORE) Investigators. *JAMA* **282,** 637–645 CrossRef Medline
21. Klinge, C. M., Jernigan, S. C., Mattingly, K. A., Risinger, K. E., and Zhang, J. (2004) Estrogen response element-dependent regulation of transcriptional activation of estrogen receptors α and β by coactivators and corepressors. *J. Mol. Endocrinol.* **33,** 387–410 CrossRef Medline
22. Wu, T. W., Chen, S., and Brinton, R. D. (2011) Membrane estrogen receptors mediate calcium signaling and MAP kinase activation in individual hippocampal neurons. *Brain Res.* **1379,** 34–43 CrossRef Medline
23. Soltysik, K., and Czekaj, P. (2013) Membrane estrogen receptors: is it an alternative way of estrogen action? *J. Physiol. Pharmacol.* **64,** 129–142 Medline
24. LoPachin, R. M., and Gavin, T. (2014) Molecular mechanisms of aldehyde toxicity: a chemical perspective. *Chem. Res. Toxicol.* **27,** 1081–1091 CrossRef Medline
25. Pinton, P., Giorgi, C., Siviero, R., Zecchini, E., and Rizzuto, R. (2008) Calcium and apoptosis: ER-mitochondria Ca^{2+} transfer in the control of apoptosis. *Oncogene* **27,** 6407–6418 CrossRef Medline
26. Zhang, J., Kiser, P. D., Badiee, M., Palczewska, G., Dong, Z., Golczak, M., Tochtrop, G. P., and Palczewski, K. (2015) Molecular pharmacodynamics of emixustat in protection against retinal degeneration. *J. Clin. Invest.* **125,** 2781–2794 CrossRef Medline

27. Yamazaki, H., Ohguro, H., Maeda, T., Maruyama, I., Takano, Y., Metoki, T., Nakazawa, M., Sawada, H., and Dezawa, M. (2002) Preservation of retinal morphology and functions in royal college surgeons rat by nilvadipine, a Ca^{2+} antagonist. *Invest. Ophthalmol. Vis. Sci.* **43,** 919–926 Medline
28. Sato, M., Ohguro, H., Ohguro, I., Mamiya, K., Takano, Y., Yamazaki, H., Metoki, T., Miyagawa, Y., Ishikawa, F., and Nakazawa, M. (2003) Study of pharmacological effects of nilvadipine on RCS rat retinal degeneration by microarray analysis. *Biochem. Biophys. Res. Commun.* **306,** 826–831 CrossRef Medline
29. Takano, Y., Ohguro, H., Dezawa, M., Ishikawa, H., Yamazaki, H., Ohguro, I., Mamiya, K., Metoki, T., Ishikawa, F., and Nakazawa, M. (2004) Study of drug effects of calcium channel blockers on retinal degeneration of rd mouse. *Biochem. Biophys. Res. Commun.* **313,** 1015–1022 CrossRef Medline
30. Takeuchi, K., Nakazawa, M., and Mizukoshi, S. (2008) Systemic administration of nilvadipine delays photoreceptor degeneration of heterozygous retinal degeneration slow (rds) mouse. *Exp. Eye Res.* **86,** 60–69 CrossRef Medline
31. Dodds, M. L., Kargacin, M. E., and Kargacin, G. J. (2001) Effects of antioestrogens and β-estradiol on calcium uptake by cardiac sarcoplasmic reticulum. *Br. J. Pharmacol.* **132,** 1374–1382 CrossRef Medline
32. Fan, H., Du, X., Zhang, J., Zheng, H., Lu, X., Wu, Q., Li, H., Wang, H., Shi, Y., Gao, G., Zhou, Z., Tan, D.-X., and Li, X. (2017) Selective inhibition of Ebola entry with selective estrogen receptor modulators by disrupting the endolysosomal calcium. *Sci. Rep.* **7,** 41226 CrossRef Medline
33. Wang, X., Zhao, L., Zhang, Y., Ma, W., Gonzalez, S. R., Fan, J., Kretschmer, F., Badea, T. C., Qian, H. H., and Wong, W. T. (2017) Tamoxifen provides structural and functional rescue in murine models of photoreceptor degeneration. *J. Neurosci.* **37,** 3294–3310 CrossRef Medline
34. Mürdter, T. E., Schroth, W., Bacchus-Gerybadze, L., Winter, S., Heinkele, G., Simon, W., Fasching, P. A., Fehm, T., German Tamoxifen and AI Clinicians Group, Eichelbaum, M., Schwab, M., and Brauch, H. (2011) Activity levels of tamoxifen metabolites at the estrogen receptor and the impact of genetic polymorphisms of phase I and II enzymes on their concentration levels in plasma. *Clin. Pharmacol. Ther.* **89,** 708–717 CrossRef Medline
35. Ning, M., Zhou, C., Weng, J., Zhang, S., Chen, D., Yang, C., Wang, H., Ren, J., Zhou, L., Jin, C., and Wang, M. W. (2007) Biological activities of a novel selective oestrogen receptor modulator derived from raloxifene (Y134). *Br. J. Pharmacol.* **150,** 19–28 CrossRef Medline
36. Gao, H., Katzenellenbogen, J. A., Garg, R., and Hansch, C. (1999) Comparative QSAR analysis of estrogen receptor ligands. *Chem. Rev.* **99,** 723–744 CrossRef Medline
37. Grese, T. A., and Dodge, J. A. (1998) Selective estrogen receptor modulators (SERMs). *Curr. Pharm. Des.* **4,** 71–92 Medline
38. Schmid, C. R., Sluka, J. P., Duke, K. M., and Glasebrook, A. W. (1999) Novel nonsteroidal selective estrogen receptor modulators: carbon and heteroatom replacement of oxygen in the ethoxypiperidine region of raloxifene. *Bioorg. Med. Chem. Lett.* **9,** 523–528 CrossRef Medline
39. Grese, T. A., Pennington, L. D., Sluka, J. P., Adrian, M. D., Cole, H. W., Fuson, T. R., Magee, D. E., Phillips, D. L., Rowley, E. R., Shetler, P. K., Short, L. L., Venugopalan, M., Yang, N. N., Sato, M., Glasebrook, A. L., and Bryant, H. U. (1998) Synthesis and pharmacology of conformationally restricted raloxifene analogues: highly potent selective estrogen receptor modulators. *J. Med. Chem.* **41,** 1272–1283 CrossRef Medline
40. Yang, C., Xu, G., Li, J., Wu, X., Liu, B., Yan, X., Wang, M., and Xie, Y. (2005) Benzothiophenes containing a piperazine side chain as selective ligands for the estrogen receptor α and their bioactivities *in vivo*. *Bioorg. Med. Chem. Lett.* **15,** 1505–1507 CrossRef Medline
41. Rattner, A., Smallwood, P. M., and Nathans, J. (2000) Identification and characterization of all-*trans*-retinol dehydrogenase from photoreceptor outer segments, the visual cycle enzyme that reduces all-*trans*-retinal to all-*trans*-retinol. *J. Biol. Chem.* **275,** 11034–11043 CrossRef Medline
42. Molday, R. S., Beharry, S., Ahn, J., and Zhong, M. (2006) Binding of *N*-retinylidene-PE to ABCA4 and a model for its transport across membranes. *Adv. Exp. Med. Biol.* **572,** 465–470 CrossRef Medline
43. Tsybovsky, Y., Wang, B., Quazi, F., Molday, R. S., and Palczewski, K. (2011) Posttranslational modifications of the photoreceptor-specific ABC transporter ABCA4. *Biochemistry* **50,** 6855–6866 CrossRef Medline
44. Kohno, H., Chen, Y., Kevany, B. M., Pearlman, E., Miyagi, M., Maeda, T., Palczewski, K., and Maeda, A. (2013) Photoreceptor proteins initiate microglial activation via Toll-like receptor 4 in retinal degeneration mediated by all-*trans*-retinal. *J. Biol. Chem.* **288,** 15326–15341 CrossRef Medline
45. Kiser, P. D., Kolesnikov, A. V., Kiser, J. Z., Dong, Z., Chaurasia, B., Wang, L., Summers, S. A., Hoang, T., Blackshaw, S., Peachey, N. S., Kefalov, V. J., and Palczewski, K. (2019) Conditional deletion of Des1 in the mouse retina does not impair the visual cycle in cones. *FASEB J.* **33,** 5782–5792 CrossRef Medline
46. Blackshaw, S., Fraioli, R. E., Furukawa, T., and Cepko, C. L. (2001) Comprehensive analysis of photoreceptor gene expression and the identification of candidate retinal disease genes. *Cell* **107,** 579–589 CrossRef Medline
47. Onishi, A., Peng, G. H., Poth, E. M., Lee, D. A., Chen, J., Alexis, U., de Melo, J., Chen, S., and Blackshaw, S. (2010) The orphan nuclear hormone receptor ERRβ controls rod photoreceptor survival. *Proc. Natl. Acad. Sci. U.S.A.* **107,** 11579–11584 CrossRef Medline
48. Giguère, V. (2002) To ERR in the estrogen pathway. *Trends Endocrinol. Metab.* **13,** 220–225 CrossRef Medline
49. Shiose, S., Chen, Y., Okano, K., Roy, S., Kohno, H., Tang, J., Pearlman, E., Maeda, T., Palczewski, K., and Maeda, A. (2011) Toll-like receptor 3 is required for development of retinopathy caused by impaired all-*trans*-retinal clearance in mice. *J. Biol. Chem.* **286,** 15543–15555 CrossRef Medline
50. Rózanowska, M., and Sarna, T. (2005) Light-induced damage to the retina: role of rhodopsin chromophore revisited. *Photochem. Photobiol.* **81,** 1305–1330 CrossRef Medline
51. Sliney, D. H. (2002) How light reaches the eye and its components. *Int. J. Toxicol.* **21,** 501–509 CrossRef Medline
52. Sliney, D. H. (2001) Photoprotection of the eye: UV radiation and sunglasses. *J. Photochem. Photobiol. B* **64,** 166–175 CrossRef Medline
53. Levin, E. R. (2008) Rapid signaling by steroid receptors. *Am. J. Physiol. Regul. Integr. Comp. Physiol.* **295,** R1425–R1430 CrossRef Medline
54. Ogueta, S. B., Schwartz, S. D., Yamashita, C. K., and Farber, D. B. (1999) Estrogen receptor in the human eye: influence of gender and age on gene expression. *Invest. Ophthalmol. Vis. Sci.* **40,** 1906–1911 Medline
55. Chen, Y., Palczewska, G., Masuho, I., Gao, S., Jin, H., Dong, Z., Gieser, L., Brooks, M. J., Kiser, P. D., Kern, T. S., Martemyanov, K. A., Swaroop, A., and Palczewski, K. (2016) Synergistically acting agonists and antagonists of G protein-coupled receptors prevent photoreceptor cell degeneration. *Sci. Signal.* **9,** ra74 CrossRef Medline
56. Parish, C. A., Hashimoto, M., Nakanishi, K., Dillon, J., and Sparrow, J. (1998) Isolation and one-step preparation of A2E and iso-A2E, fluorophores from human retinal pigment epithelium. *Proc. Natl. Acad. Sci. U.S.A.* **95,** 14609–14613 CrossRef Medline
57. He, M., Du, W., Du, Q., Zhang, Y., Li, B., Ke, C., Ye, Y., and Du, Q. (2013) Isolation of the retinal isomers from the isomerization of all-*trans*-retinal by flash countercurrent chromatography. *J. Chromatogr. A* **1271,** 67–70 CrossRef Medline
58. Kiser, P. D., Zhang, J., Badiee, M., Li, Q., Shi, W., Sui, X., Golczak, M., Tochtrop, G. P., and Palczewski, K. (2015) Catalytic mechanism of a retinoid isomerase essential for vertebrate vision. *Nat. Chem. Biol.* **11,** 409–415 CrossRef Medline
59. He, J. S., Soo, P., Evers, M., Parsons, K. M., Hein, N., Hannan, K. M., Hannan, R. D., and George, A. J. (2018) High-content imaging approaches to quantitate stress-induced changes in nucleolar morphology. *Assay Drug. Dev. Technol.* **16,** 320–332 CrossRef Medline
60. Crouch, S. P., Kozlowski, R., Slater, K. J., and Fletcher, J. (1993) The use of ATP bioluminescence as a measure of cell proliferation and cytotoxicity. *J. Immunol. Methods* **160,** 81–88 CrossRef Medline
61. Kangas, L., Grönroos, M., and Nieminen, A. L. (1984) Bioluminescence of cellular ATP: a new method for evaluating cytotoxic agents *in vitro*. *Med. Biol.* **62,** 338–343 Medline

62. Lock, J. T., Parker, I., and Smith, I. F. (2015) A comparison of fluorescent Ca^{2+} indicators for imaging local Ca^{2+} signals in cultured cells. *Cell Calcium* **58,** 638–648 CrossRef Medline
63. Zhang, J. H., Chung, T. D., and Oldenburg, K. R. (1999) A simple statistical parameter for use in evaluation and validation of high throughput screening assays. *J. Biomol. Screen.* **4,** 67–73 CrossRef Medline
64. Huber, G., Beck, S. C., Grimm, C., Sahaboglu-Tekgoz, A., Paquet-Durand, F., Wenzel, A., Humphries, P., Redmond, T. M., Seeliger, M. W., and Fischer, M. D. (2009) Spectral domain optical coherence tomography in mouse models of retinal degeneration. *Invest. Ophthalmol. Vis. Sci.* **50,** 5888–5895 CrossRef Medline
65. Reznicek, L., Stumpf, C., Seidensticker, F., Kampik, A., Neubauer, A. S., and Kernt, M. (2014) Role of wide-field autofluorescence imaging and scanning laser ophthalmoscopy in differentiation of choroidal pigmented lesions. *Int. J. Ophthalmol.* **7,** 697–703 CrossRef Medline
66. Maeda, A., Maeda, T., Imanishi, Y., Kuksa, V., Alekseev, A., Bronson, J. D., Zhang, H., Zhu, L., Sun, W., Saperstein, D. A., Rieke, F., Baehr, W., and Palczewski, K. (2005) Role of photoreceptor-specific retinol dehydrogenase in the retinoid cycle *in vivo*. *J. Biol. Chem.* **280,** 18822–18832 CrossRef Medline
67. Zheng, G. X., Terry, J. M., Belgrader, P., Ryvkin, P., Bent, Z. W., Wilson, R., Ziraldo, S. B., Wheeler, T. D., McDermott, G. P., Zhu, J., Gregory, M. T., Shuga, J., Montesclaros, L., Underwood, J. G., Masquelier, D. A., *et al.* (2017) Massively parallel digital transcriptional profiling of single cells. *Nat. Commun.* **8,** 14049 CrossRef Medline
68. Butler, A., Hoffman, P., Smibert, P., Papalexi, E., and Satija, R. (2018) Integrating single-cell transcriptomic data across different conditions, technologies, and species. *Nat. Biotechnol.* **36,** 411–420 CrossRef Medline
69. Bray, M. A., and Carpenter, A. (2004) Advanced assay development guidelines for image-based high content screening and analysis. in *Assay Guidance Manual* (Sittampalam, G. S., Coussens, N. P., Brimacombe, K., Grossman, A., Arkin, M., Auld, D., Austin, C., Baell, J., Bejcek, B., Caaveiro, J. M. M., Chung, T. D. Y., Dahlin, J. L., Devanaryan, V., Foley, T. L., Glicksman, M., *et al.*, eds), Bethesda, MD
70. Kittelson, J. M. (2011) A Review of: "Fundamentals of Biostatistics, 7th ed., by B. Rosner". *J. Biopharmaceutical Statistics* **21,** 1046–1048 CrossRef